

# Charge Loss Correction in the Silicon-Tungsten Tracker-Converter for Proton-Helium Charge Identification in the DAMPE Detector

Arshia Ruina,<sup>a,\*</sup> Mikhail Stolpovskiy,<sup>a</sup> Maksym Deliyergiyev<sup>a</sup> and Yuxing Cui<sup>b</sup> on behalf of the DAMPE Collaboration

(a complete list of authors can be found at the end of the proceedings)

<sup>a</sup>*Département de physique nucléaire et corpusculaire, University of Geneva, Quai Ernest-Ansermet 24, 1205 Geneva, Switzerland*

<sup>b</sup>*Key Laboratory of Dark Matter and Space Astronomy, Purple Mountain Observatory, Chinese Academy of Sciences, Nanjing 210033, China*  
E-mail: [arshia.ruina@unige.ch](mailto:arshia.ruina@unige.ch), [mikhail.stolpovskiy@unige.ch](mailto:mikhail.stolpovskiy@unige.ch), [maksym.deliyergiyev@unige.ch](mailto:maksym.deliyergiyev@unige.ch), [yxcui@pmo.ac.cn](mailto:yxcui@pmo.ac.cn)

The DArk Matter Particle Explorer (DAMPE) is a satellite-borne experiment, in operation since 2015, aimed at studying high-energy gamma rays and cosmic nuclei fluxes. Of the various sub-detectors in the DAMPE payload, the Silicon-Tungsten tracKer-converter (STK) plays a significant role in the charge measurement of incoming ions. Depending on the angle of inclination of the impinging particle and its position of impact on these strips, the collected charge can spread between the strips which results in some fractional signal loss. The  $\eta$  variable is used to identify this spread of charge across the strips and correct for the associated charge loss. This brings us closer to accurate determination of particle charge which is crucial for ensuring a good discrimination between particles. The  $\eta$ -correction is, therefore, expected to play an important role in the determination of heavy ions by the DAMPE detector. It has helped reduce the proton background for the helium identification in STK by a factor of 1.5 for MIP tracks. It has been successfully applied to carbon nuclei and its application to heavier nuclei is currently being studied.

37<sup>th</sup> International Cosmic Ray Conference (ICRC 2021)  
July 12th – 23rd, 2021  
Online – Berlin, Germany

---

\*Presenter

## 1. The Silicon-Tungsten Tracker

The DAMPE detector comprises four sub-detector modules: the plastic scintillator detector (PSD) for charge measurement, the silicon-tungsten tracker-converter (STK) for trajectory measurement, the bismuth-germanium-oxide (BGO) electromagnetic calorimeter for energy measurement and a neutron detector (NUD) for electron-hadron discrimination.

The working principle of the STK is similar to those in previous experiments like Fermi and Agile where incident photons undergo conversion into electron-positron pairs in the tungsten layers and are subsequently detected in the silicon layers. The STK is made of six tracking planes, each consisting of a double layer of silicon micro-strip detectors (SSDs) to measure the X- and Y-coordinates of the incident particle track. A sensor module is made up of 4 of these single-sided AC-coupled SSDs and is called a ladder (figure 1). 16 ladders are arranged on each tracking layer as shown in figure 2 rendering a total of 192 ladders in the STK. The tracking planes 2, 3 and 4 have tungsten plates inserted between them for photon conversion. The silicon sensors are segmented into 768 p-doped strips in an n-doped bulk and read-out is done only for every other strip to regulate the power consumption, electronics density and data transfer [2]. A detailed description of the STK construction and its performance on orbit are reported in [3].

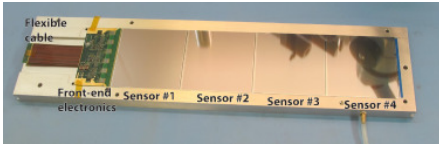


**Figure 1:** The silicon ladder is made of four silicon micro-strip detectors. The front-end electronics is located at one extremity of the ladder which reads out 384 strips using 6 VA140 chips. Figure taken from [2].

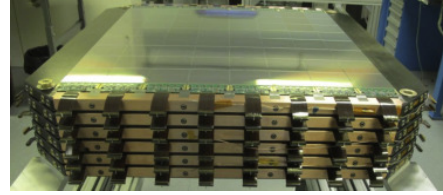


**Figure 2:** The STK before the assembly of the last tray. 16 ladders (consisting of 64 silicon detectors) are visible here. Figure taken from [2].

## 2. Charge Measurement in the STK

The energy deposited by particles incident on the STK sensors is measured from the signal recorded by one or several read-out strips on the ladders. A pre-built algorithm finds what we call clusters of the signal, which when associated with a track, give us information on the charge. By definition, a cluster is formed with at least one channel that has a signal larger than 4 times the channel noise and neighbouring channels with signal larger than 1.5 times the channel noise. Each channel signal is then summed up to give the cluster charge in units of ADC counts. From the Bethe-Bloch equation, we know that the average energy loss of a particle  $\langle \frac{dE}{dx} \rangle$  is proportional to its squared charge ( $z^2$ ). However, in order to obtain the charge and to be able to discriminate between particles of different charges, it is important to calibrate the STK ladders first. One such calibration method is to correct for the cluster amplitude's dependence on the impact point and inclination of the incident particle with respect to the sensor, also known as the charge-loss correction.

### 3. Correction for the Charge Loss

In order to distinguish between signals generated by particles impinging on the read-out and floating strips of the STK ladder, the  $\eta$  variable is introduced and defined as

$$\eta = \frac{S_1}{S_1 + S_2}, \quad (1)$$

where  $S_1$  and  $S_2$  are signals from two adjacent channels with  $S_1$  being the highest and  $S_2$  being the next highest signals. A schematic to understand the justification of using this variable is shown in figure 3. The definition given here allows the value of  $\eta$  to range between 0.5 (when two of the neighbouring read-out strips associated to a cluster have the same value of signal) and 1 (when it is a single-strip cluster).

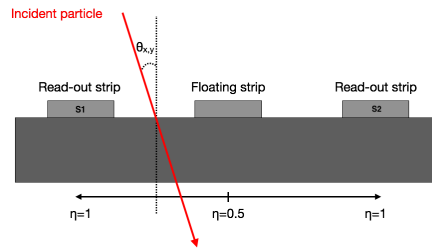


**Figure 3:** Schematic cross-sectional view of two consecutive strips (alternating read-out and floating strips) on the STK ladder, representing the correlation between  $\eta$  and the impact point of the particle.

For the purpose of developing this correction, both, flight data from the period 2015-2020 and MC simulated data, were used. Event selection is the same as in [4] and high quality tracks that pass through all layers of the STK are selected. A distribution of the  $\eta$ -variable is shown in figure 4 and the dependance of the STK cluster energy (in ADC counts) on  $\eta$  is shown in figure 5.

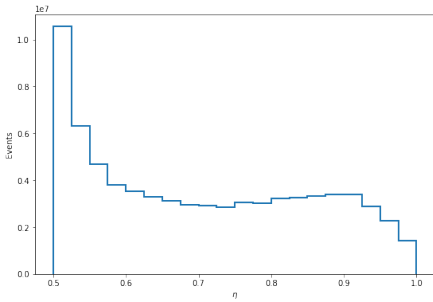


**Figure 4:**  $\eta$ -distribution for flight data for  $0.5 < \eta < 1$ .

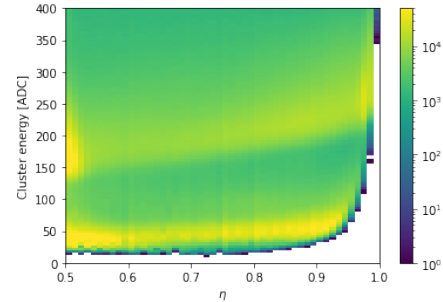


**Figure 5:** STK cluster charge distribution as a function of  $\eta$ .

The loss of charge is evident as the impact position varies (which is quantified by  $\eta$ ) for both, proton and helium candidates. The same distribution, in bins of the angle of inclination in STK, where  $\theta_{x,y} \in (0^\circ, 40^\circ)$  and each bin corresponds to a step of  $5^\circ$  in  $\theta_{x,y}$ , is shown in figure 6. From this, we can see that the charge loss is less for higher inclinations. This can be attributed to the fact that the charge in these cases gets spread over a larger number of strips which compensates for the loss and attenuates the effect.

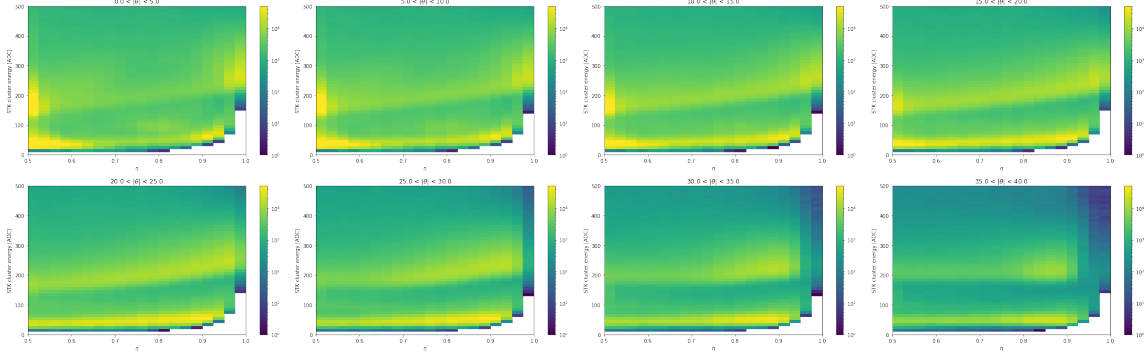


**Figure 6:** STK cluster charge distribution as a function of  $\eta$ , in bins of the angle of inclination in STK,  $\theta_{x,y} \in (0^\circ, 40^\circ)$ , where each sub-figure corresponds to a bin size of  $5^\circ$

The  $\eta$ -correction was revised and improved by including the dependance of the STK signal on the number of strips (shown in figure 7) that constitute a cluster. [1]

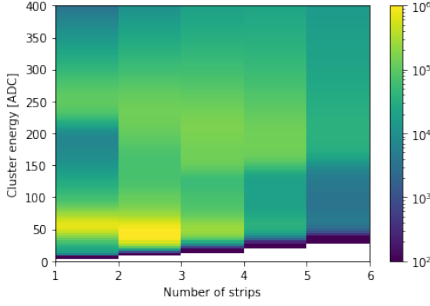


**Figure 7:** STK cluster charge distribution as a function of the number of strips that form a STK cluster

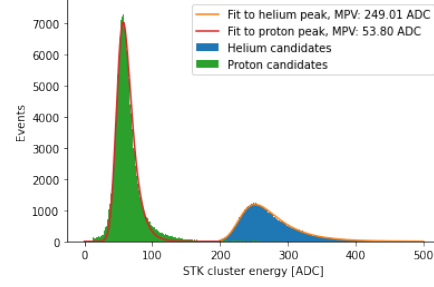


**Figure 8:** Moyal fits made to the STK energy for proton and helium candidates (selected using PSD charge) for single-strip clusters give us the target values for the charge loss correction.

In the case of single-strip clusters where the charge is not shared between strips and  $\eta = 1$ , a correction is not required and therefore, the energy of single-strip clusters is used as the target energy for the correction for all inclinations as shown in figure 8. Here, the proton and helium candidates were chosen after placing a selection cut on the PSD energy. Moyal fits were made to each peak and the most probable value (MPV) is set as the target energies – 53.80 ADC for proton clusters and 249.01 ADC for helium.

The correction is developed in the following way: First, the STK cluster energy histograms for the pre-selected helium candidates are built in bins of number of strips (that make up an charge cluster in the STK),  $\theta_{x,y}$  and  $\eta$ . For a given bin in  $\eta$ , these histograms are fitted with a Moyal distribution (with a linear background). One such distribution and fit is shown in figure 9 and we obtain MPVs for these fits in each  $\eta$  bin. For each combination of bins in  $\theta_{x,y}$  and number of strips, a 2D distribution of the dependance of the STK energy on  $\eta$  is obtained (see figure 10) where the MPVs of the distributions in slices of  $\eta$  are marked in black dots. The dependancy of these MPVs on  $\eta$  are fitted using a quadratic function

$$f(\theta_{x,y}, n_{strips}) = a\eta^2 + b\eta + c \quad (2)$$

whose the quadratic coefficient  $a$  fixed at 200. The linear and constant terms,  $b$  and  $c$ , of these functions are determined from their dependance on  $\theta_{x,y}$  in bins of number of strips, shown in figure 11. The correction parameter for a given bin in  $\eta$  is given by

$$\text{Correction param.}(\eta) = \frac{E_{\text{He, 1-strip}}}{f(\theta_{x,y}, n_{\text{strips}})} \quad (3)$$

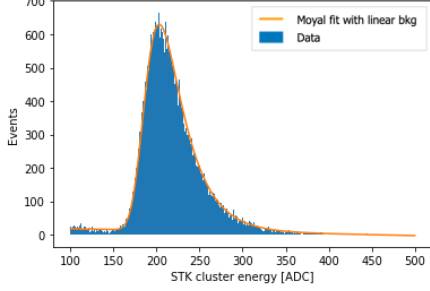


**Figure 9:** STK energy for clusters with  $0.8 < \eta < 0.85$ ,  $23.33^\circ < |\theta| < 29.17^\circ$  and number of strips that make up the cluster = 2.

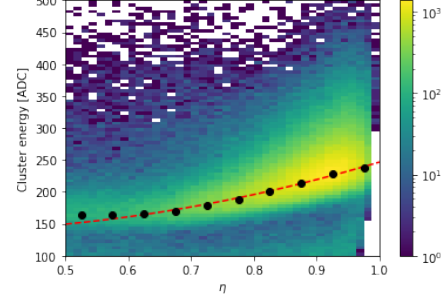


**Figure 10:** A 2D distribution of the STK cluster energy vs.  $\eta$  in the bin  $23.33^\circ < |\theta| < 29.17^\circ$  and for number of strips that make up the cluster = 2.

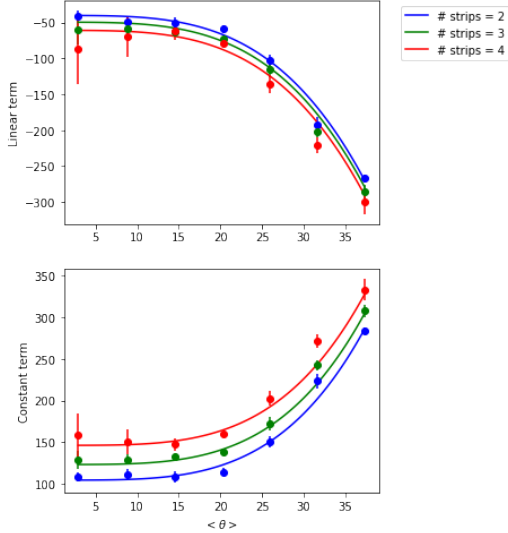


**Figure 11:** Linear and constant terms of the correction functions for different values of  $\theta_{x,y}$  and number of strips

and after the correction. A ratio between the sigma and MPV of these fits is shown in figures 13 and 14. Template fits were made to MC data in bins of deposited energy in the BGO and signal regions for proton and helium were defined. An example of such a fit is shown in figure 15. The background contamination in the proton and helium signal regions is computed using MC simulated data. These contamination percentages are shown in figures 16 and 17 which show a clear reduction in background after the charge loss correction.

where  $E_{\text{He, 1-strip}}$  is the target value of the cluster charge, which is the MPV of STK energy of helium for single-strip clusters and the denominator is the analytical function for evaluated for a given  $\eta$ . The correction parameters were applied to the STK cluster charge for every STK ladder in the following way:

$$E_{\text{corr}} = E \times \text{Correction param.}(\eta) \quad (4)$$

#### 4. Results

The distributions of the STK cluster charge after eta correction is shown in various bins of  $\theta$  in figure 12. The reduction in charge loss is evident when compared with figure 6. Fits were made to the STK energy distributions in bins of energy deposited in the BGO for both, helium and proton candidates, before

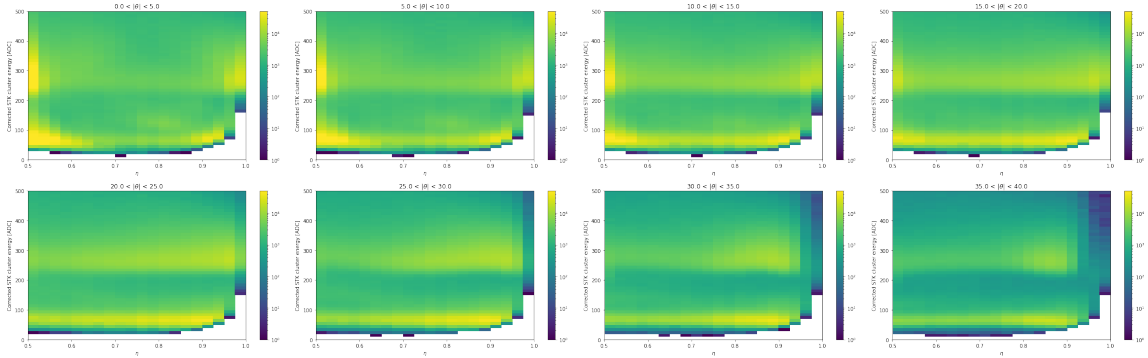


**Figure 12:** STK cluster charge distribution after eta correction, as a function of  $\eta$ , in bins of the angle of inclination in STK,  $\theta_{x,y} \in (0^\circ, 40^\circ)$ , where each sub-figure corresponds to a bin size of  $5^\circ$ .

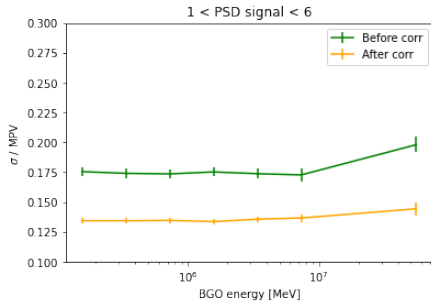


**Figure 13:**  $\sigma$ /MPV ratios for proton candidates in the BGO energy bins. A reduction in the values post correction indicates improvement in the peak positions.

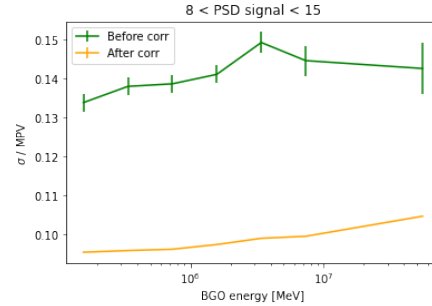


**Figure 14:**  $\sigma$ /MPV ratios for helium candidates in the BGO energy bins. A reduction in the values post correction indicates improvement in the peak positions.

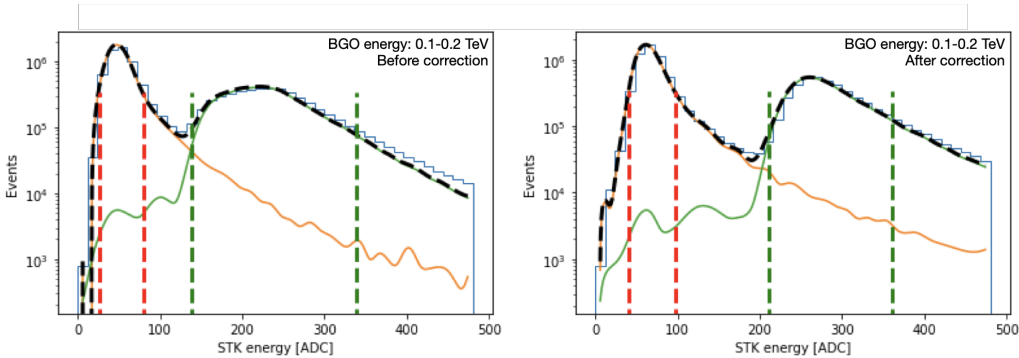


**Figure 15:** STK energy for flight data (in blue) and template fits to proton (in orange) and helium (in green) MC data in BGO energy bin 0.1-0.2 TeV before (left) and after (right) charge loss correction. The black dashed line is the sum of the template fits. The vertical dashed lines denote the signal region for proton (in red) and helium (in green) where the contamination percentages were computed.

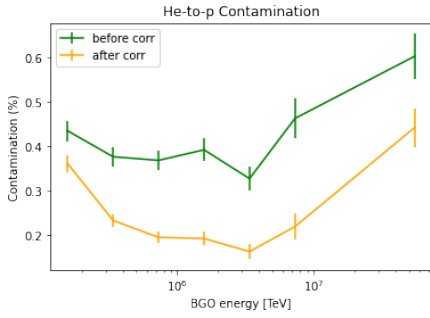


**Figure 16:** Helium contamination percentages under the proton peak as a function of BGO energy

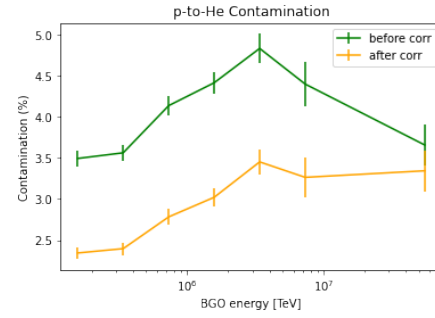


**Figure 17:** Proton contamination percentages under the helium peak as a function of BGO energy

## 5. Conclusion

A charge loss correction or eta correction, that includes the dependance of the STK cluster energy on the position of impact and angle of inclination of the incident particle and the number of strips that make up a charge cluster, was developed and deployed. This correction reduces the proton background for helium identification by a factor of 1.5 for MIP tracks and is, therefore, important for charge selection and identification with the STK. The correction was also successfully applied to carbon nuclei and is open to adaptation for heavier ions. In the case of heavier ions, very high energy deposition in the STK clusters results in the saturation of the readout electronics, thereby significantly decreasing the MPV of peaks, especially at  $\eta \sim 1$ . A development of the new eta correction that takes this effect into account is currently underway.

## 6. Acknowledgements

The DAMPE mission is funded by the strategic priority science and technology projects in space science of Chinese Academy of Sciences. In China the data analysis was supported in part by the National Key Research and Development Program of China (No. 2016YFA0400200), the National Natural Science Foundation of China (Nos. 11525313, 11622327, 11722328, U1738133, U1738205, U1738207, U1738208), the strategic priority science and technology projects of Chinese Academy of Sciences (No. XDA15051100), the 100 Talents Program of Chinese Academy of Sciences, and the Young Elite Scientists Sponsorship Program. In Europe the activities and the data analysis are supported by the Swiss National Science Foundation (SNSF), Switzerland; the National Institute for Nuclear Physics (INFN), Italy.

## References

- [1] S. Vitillo and V. Gallo (on behalf of the DAMPE collaboration) *Measurement of cosmic-ray charge with the DAMPE Silicon-Tungsten Tracker* in proceedings of The 35th International Cosmic Ray Conference, PoS(ICRC2017)240.
- [2] P. Azzarello et al. *The DAMPE Silicon-Tungsten Tracker* in Nuclear Instruments and Methods in Physics Research A 831 (2016) 378-384.

- [3] V. Gallo et al. *The DAMPE silicon tungsten tracker* in proceedings of The 25th International Workshop on Vertex Detectors, PoS(Vertex2016)010.
- [4] F. Alemanno et al. (DAMPE collaboration) *Measurement of the cosmic ray helium energy spectrum from 70 GeV to 80 TeV with the DAMPE space mission* in Phys. Rev. Lett. 126. 201102 (2021).

**Full Authors List: DAMPE Collaboration**

F. Alemanno<sup>1,2</sup>, Q. An<sup>3,4</sup>, P. Azzarello<sup>5</sup>, F. C. T. Barbato<sup>1,2</sup>, P. Bernardini<sup>6,7</sup>, X. J. Bi<sup>8,9</sup>, M. S. Cai<sup>10,11</sup>, E. Casilli<sup>6,7</sup>, E. Catanzani<sup>12</sup>, J. Chang<sup>10,11</sup>, D. Y. Chen<sup>10</sup>, J. L. Chen<sup>13</sup>, Z. F. Chen<sup>10,11</sup>, M. Y. Cui<sup>10</sup>, T. S. Cui<sup>14</sup>, Y. X. Cui<sup>10,11</sup>, H. T. Dai<sup>3,4</sup>, A. De Benedittis<sup>6,7</sup>, I. De Mitri<sup>1,2</sup>, F. de Palma<sup>6,7</sup>, M. Deliyergiyev<sup>5</sup>, M. Di Santo<sup>1,2</sup>, Q. Ding<sup>10,11</sup>, T. K. Dong<sup>10</sup>, Z. X. Dong<sup>14</sup>, G. Donvito<sup>15</sup>, D. Droz<sup>5</sup>, J. L. Duan<sup>13</sup>, K. K. Duan<sup>10</sup>, D. D'Urso<sup>12,1</sup>, R. R. Fan<sup>8</sup>, Y. Z. Fan<sup>10,11</sup>, K. Fang<sup>8</sup>, F. Fang<sup>13</sup>, C. Q. Feng<sup>3,4</sup>, L. Feng<sup>10</sup>, P. Fusco<sup>15,16</sup>, M. Gao<sup>8</sup>, F. Gargano<sup>15</sup>, K. Gong<sup>8</sup>, Y. Z. Gong<sup>10</sup>, D. Y. Guo<sup>8</sup>, J. H. Guo<sup>10,11</sup>, S. X. Han<sup>14</sup>, Y. M. Hu<sup>10</sup>, G. S. Huang<sup>3,4</sup>, X. Y. Huang<sup>10,11</sup>, Y. Y. Huang<sup>10</sup>, M. Ionica<sup>12</sup>, W. Jiang<sup>10</sup>, J. Kong<sup>13</sup>, A. Kotenko<sup>5</sup>, D. Kyrtzsis<sup>1,2</sup>, S. J. Lei<sup>10</sup>, W. H. Li<sup>10,11</sup>, W. L. Li<sup>14</sup>, X. Li<sup>10</sup>, X. Q. Li<sup>14</sup>, Y. M. Liang<sup>14</sup>, C. M. Liu<sup>3,4</sup>, H. Liu<sup>10</sup>, J. Liu<sup>13</sup>, S. B. Liu<sup>3,4</sup>, Y. Liu<sup>10</sup>, F. Loparco<sup>15,16</sup>, C. N. Luo<sup>10,11</sup>, M. Ma<sup>14</sup>, P. X. Ma<sup>10</sup>, T. Ma<sup>10</sup>, X. Y. Ma<sup>14</sup>, G. Marsella<sup>6,7,2</sup>, M. N. Mazziotta<sup>15</sup>, D. Mo<sup>13</sup>, X. Y. Niu<sup>13</sup>, X. Pan<sup>10,11</sup>, A. Parenti<sup>1,2</sup>, W. X. Peng<sup>8</sup>, X. Y. Peng<sup>10</sup>, C. Perrina<sup>5,3</sup>, R. Qiao<sup>8</sup>, J. N. Rao<sup>14</sup>, A. Ruina<sup>5</sup>, M. M. Salinas<sup>5</sup>, G. Z. Shang<sup>14</sup>, W. H. Shen<sup>14</sup>, Z. Q. Shen<sup>10</sup>, Z. T. Shen<sup>3,4</sup>, L. Silveri<sup>1,2</sup>, J. X. Song<sup>14</sup>, M. Stolpovskiy<sup>5</sup>, H. Su<sup>13</sup>, M. Su<sup>17</sup>, H. R. Sun<sup>3,4</sup>, Z. Y. Sun<sup>13</sup>, A. Surdo<sup>7</sup>, X. J. Teng<sup>14</sup>, A. Tykhonov<sup>5</sup>, H. Wang<sup>14</sup>, J. Z. Wang<sup>8</sup>, L. G. Wang<sup>14</sup>, S. Wang<sup>10</sup>, S. X. Wang<sup>10</sup>, X. L. Wang<sup>3,4</sup>, Y. Wang<sup>3,4</sup>, Y. F. Wang<sup>3,4</sup>, Y. Z. Wang<sup>10</sup>, D. M. Wei<sup>10,11</sup>, J. J. Wei<sup>10</sup>, Y. F. Wei<sup>3,4</sup>, D. Wu<sup>8</sup>, J. Wu<sup>10,11</sup>, L. B. Wu<sup>1,2</sup>, S. S. Wu<sup>14</sup>, X. Wu<sup>5</sup>, Z. Q. Xia<sup>10</sup>, H. T. Xu<sup>14</sup>, Z. H. Xu<sup>10,11</sup>, Z. L. Xu<sup>10</sup>, E. H. Xu<sup>3,4</sup>, Z. Z. Xu<sup>3,4</sup>, G. F. Xue<sup>14</sup>, H. B. Yang<sup>13</sup>, P. Yang<sup>13</sup>, Y. Q. Yang<sup>13</sup>, H. J. Yao<sup>13</sup>, Y. H. Yu<sup>13</sup>, G. W. Yuan<sup>10,11</sup>, Q. Yuan<sup>10,11</sup>, C. Yue<sup>10</sup>, J. J. Zang<sup>10,4</sup>, S. X. Zhang<sup>13</sup>, W. Z. Zhang<sup>14</sup>, Yan Zhang<sup>10</sup>, Yi Zhang<sup>10,11</sup>, Y. J. Zhang<sup>13</sup>, Y. L. Zhang<sup>3,4</sup>, Y. P. Zhang<sup>13</sup>, Y. Q. Zhang<sup>10</sup>, Z. Zhang<sup>10</sup>, Z. Y. Zhang<sup>3,4</sup>, C. Zhao<sup>3,4</sup>, H. Y. Zhao<sup>13</sup>, X. F. Zhao<sup>14</sup>, C. Y. Zhou<sup>14</sup>, and Y. Zhu<sup>14</sup>

<sup>1</sup>Gran Sasso Science Institute (GSSI), Via Iacobucci 2, I-67100 L'Aquila, Italy

<sup>2</sup>Istituto Nazionale di Fisica Nucleare (INFN) -Laboratori Nazionali del Gran Sasso, I-67100 Assergi, L'Aquila, Italy

<sup>3</sup>State Key Laboratory of Particle Detection and Electronics, University of Science and Technology of China, Hefei 230026, China

<sup>4</sup>Department of Modern Physics, University of Science and Technology of China, Hefei 230026, China

<sup>5</sup>Department of Nuclear and Particle Physics, University of Geneva, CH-1211, Switzerland

<sup>6</sup>Dipartimento di Matematica e Fisica E. De Giorgi, Università del Salento, I-73100, Lecce, Italy

<sup>7</sup>Istituto Nazionale di Fisica Nucleare (INFN) - Sezione di Lecce, I-73100, Lecce, Italy

<sup>8</sup>Institute of High Energy Physics, Chinese Academy of Sciences, Yuquan Road 19B, Beijing 100049, China

<sup>9</sup>University of Chinese Academy of Sciences, Yuquan Road 19A, Beijing 100049, China

<sup>10</sup>Key Laboratory of Dark Matter and Space Astronomy, Purple Mountain Observatory, Chinese Academy of Sciences, Nanjing 210023, China

<sup>11</sup>School of Astronomy and Space Science, University of Science and Technology of China, Hefei 230026, China

<sup>12</sup>Istituto Nazionale di Fisica Nucleare (INFN) - Sezione di Perugia, I-06123 Perugia, Italy

<sup>13</sup>Institute of Modern Physics, Chinese Academy of Sciences, Nanchang Road 509, Lanzhou 730000, China

<sup>14</sup>National Space Science Center, Chinese Academy of Sciences, Nanertiao 1, Zhongguancun, Haidian district, Beijing 100190, China

<sup>15</sup>Istituto Nazionale di Fisica Nucleare (INFN) - Sezione di Bari, I-70125, Bari, Italy

<sup>16</sup>Dipartimento di Fisica "M. Merlin" dell'Università e del Politecnico di Bari, I-70126, Bari, Italy

<sup>17</sup>Department of Physics and Laboratory for Space Research, the University of Hong Kong, Pok Fu Lam, Hong Kong SAR, China

<sup>1</sup>Now at Dipartimento di Chimica e Farmacia, Università di Sassari, I-07100, Sassari, Italy.

<sup>2</sup>Now at Dipartimento di Fisica e Chimica "E. Segre", Università degli Studi di Palermo, via delle Scienze ed. 17, I-90128 Palermo, Italy.

<sup>3</sup>Also at Institute of Physics, Ecole Polytechnique Federale de Lausanne (EPFL), CH-1015 Lausanne, Switzerland.

<sup>4</sup>Also at School of Physics and Electronic Engineering, Linyi University, Linyi 276000, China.